



HAL
open science

Analysis of TerraSAR-X data sensitivity to bare soil moisture, roughness, composition and soil crust

Maelle Aubert, Nicolas Baghdadi, Mehrez Zribi, A. Douaoui, Cécile Loumagne, Frédéric Baup, Mohammad El Hajj, Sébastien Garrigues

► **To cite this version:**

Maelle Aubert, Nicolas Baghdadi, Mehrez Zribi, A. Douaoui, Cécile Loumagne, et al.. Analysis of TerraSAR-X data sensitivity to bare soil moisture, roughness, composition and soil crust. *Remote Sensing of Environment*, 2011, 115, p. 1801 - p. 1810. 10.1016/j.rse.2011.02.021 . hal-00602355

HAL Id: hal-00602355

<https://hal.science/hal-00602355>

Submitted on 22 Jun 2011

HAL is a multi-disciplinary open access archive for the deposit and dissemination of scientific research documents, whether they are published or not. The documents may come from teaching and research institutions in France or abroad, or from public or private research centers.

L'archive ouverte pluridisciplinaire **HAL**, est destinée au dépôt et à la diffusion de documents scientifiques de niveau recherche, publiés ou non, émanant des établissements d'enseignement et de recherche français ou étrangers, des laboratoires publics ou privés.

1 **Characterization of the soil surface by TerraSAR-X imagery**

2

3 **M. Aubert⁽¹⁾, N. Baghdadi⁽¹⁾, M. Zribi⁽²⁾, A. Douaoui⁽³⁾, C. Loumagne⁽⁴⁾, F. Baup⁽²⁾, M. El Hajj⁽⁵⁾, S. Garrigues⁽⁶⁾**

4

5 ⁽¹⁾*CEMAGREF – UMR TETIS, 34196 Montpellier (France), Email: nicolas.baghdadi@teledetection.fr; maelle.aubert@teledetection.fr, tel : + 33 4*
6 *67 54 87 07*

7 ⁽²⁾*CESBIO, 31401 Toulouse (France), Email : Mehrez.Zribi@latmos.ipsl.fr; frederic.baup@cesbio.cnes.fr*

8 ⁽³⁾*Laboratoire Eau, roche et plante, Centre universistaire de Khémis miliana, 44225 (Algérie), Email : abdouaoui@yahoo.fr*

9 ⁽⁴⁾*CEMAGREF – UR HBAN, 92163 Antony (France), Email : cecile.loumagne@cemagref.fr*

10 ⁽⁵⁾*NOVELTIS, 31520 Ramonville-Saint Agne (France), Email : mahmoud.elhajj@noveltis.fr*

11 ⁽⁶⁾*CNES, 31000 Toulouse (France), Email: sebastien.garrigues@cnes.fr*

12

13 **Corresponding author:**

14 **Maëlle Aubert**

15 **500 rue Jean-François Breton, 34093 Montpellier Cedex 5, France**

16 **Tel : +33 4.67.54.87.54**

17 **Fax: +33 4.67.54.87.00 (France)**

18 **Email : maelle.aubert@teledetection.fr**

19

20

20 **ABSTRACT**

21 Soils play a key role in shaping the environment and in risk assessment. We characterized the soils
22 of bare agricultural plots using TerraSAR-X (9.5 GHz) data acquired in 2009 and 2010. We
23 analyzed the behavior of the TerraSAR-X signal for two configurations, HH-25° and HH-50°, with
24 regard to several soil conditions: moisture content, surface roughness, soil composition and soil-
25 surface structure (slaking crust).

26 The TerraSAR-X signal was more sensitive to soil moisture at a low (25°) incidence angle than at
27 a high incidence angle (50°). For high soil moisture (>25%), the TerraSAR-X signal was more
28 sensitive to soil roughness at a high incidence angle (50°) than at a low incidence angle (25°).

29 The high spatial resolution of the TerraSAR-X data (1 m) enabled the soil composition and slaking
30 crust to be analyzed at the within-plot scale based on the radar signal. The two loamy-soil
31 categories that composed our training plots did not differ sufficiently in their percentages of sand
32 and clay to be discriminated by the X-band radar signal.

33 However, the TerraSAR-X signal has the potential to detect low variations of soil moisture at the
34 within-plot scale. Consequently, the spatial distribution of slaking crust could be detected when
35 soil moisture variation is observed between soil crusted and soil without crust. Indeed, areas
36 covered by slaking crust could have greater soil moisture and consequently a greater
37 backscattering signal than soils without crust.

38

39 **Keywords:** *soil moisture, roughness, soil composition, slaking crust, X-band, TerraSAR-X images,*
40 *within field plot scale.*

41

42

42 1. INTRODUCTION

43 Floods, drought and erosion are major issues for risk assessment. In the context of sustainable
44 development, soil management is important for environmental and socioeconomic applications.
45 Hence, there is a need for continuous information about key soil parameters to predict and
46 understand these natural hazards [Wu & Wang, 2007]. Slaking crust (the disintegration of
47 ploughed clods) is a key factor that controls runoff and erosion because of its influence on
48 infiltration capacity [Cazenave & Valentin, 1992; Govers et al., 2000; King & Le Bissonnais,
49 1992; Le Bissonnais & Singer, 1992]. Similarly, by conditioning the distribution of rainfall
50 between infiltration, surface retention and runoff [Auzet et al., 2005; Cerdan et al., 2002; Valentin,
51 2005], soil moisture and surface roughness play an important role in risk assessment [Loumagne et
52 al., 1991, 2001; Oudin et al., 2003]. Nevertheless, monitoring and modeling these soil surface
53 characteristics remain difficult because of their substantial variation over space and time [Boiffin
54 et al., 1988; Brown et al., 1990; Zobeck & Onstad, 1987].

55 In this context, satellite imagery is a powerful tool that can provide accurate and repetitive spatial
56 data. Synthetic-aperture radar (SAR) techniques are particularly useful because they make it
57 possible to monitor soil parameters under any weather conditions [Dobson & Ulaby, 1986; Fung,
58 1994; Hallikainen et al., 1985; Ulaby et al., 1986]. For bare agricultural soils, the backscattered
59 radar signal depends strongly on the geometric characteristics (roughness) and dielectric properties
60 (moisture content, soil composition) of the soil. Many studies using data collected by space and
61 airborne SAR scatterometers and model simulations have already shown the potential of radar data
62 to retrieve soil parameters (roughness and moisture) [Baghdadi et al., 2002, 2006, 2007, 2008b;
63 Dobson & Ulaby, 1986; Fung et al., 1992; Holah et al., 2005; Le Hegarat et al., 2002; Oh, 2004;
64 Shi et al., 1997; Srivastava et al., 2003-2009; Ulaby et al., 1978; Zribi et al., 2005; Zribi &
65 Dechambre, 2002].

66 Whatever the SAR configuration, the radar signal follows a logarithmic function with the soil-
67 surface roughness [Fung, 1994; Ulaby et al., 1986]. Ulaby et al. (1978) have shown that the
68 influence of surface roughness decreases with increasing radar frequency. The dynamics of the
69 relationship between the radar signal and roughness parameter are stronger in the L-band than in
70 the C- and X-bands [Baghdadi et al., 2008a; Ulaby et al., 1986] Moreover, SAR data are more
71 sensitive to soil roughness at high incidence angles [Baghdadi et al., 2008a, 2008b; Zribi &
72 Dechambre, 2002].

73 The SAR signal increases with increasing soil moisture for values between 0 and 35-40%
74 [Baghdadi et al., 2007; Holah et al., 2005]. Beyond this threshold, the backscattering coefficient
75 becomes constant and then decreases with increasing soil moisture [Holah et al., 2005]. Several
76 studies in the C-band, with the SAR configuration fixed at a single polarization, have shown that
77 the sensitivity of the radar signal to soil moisture is greater at low and medium incidence angles
78 than at high incidence angles (approximately 0.2 dB/% for HH-20°-37° and approximately 0.1
79 dB/% for HH-39°) [Baghdadi et al., 2006, 2008b; Beaudoin et al., 1990; Srivastava et al., 2003;
80 Zribi & Dechambre, 2002].

81 However, few studies have been conducted in the X-band. The first results based on microwave
82 measurements in the X-band have shown that an incidence angle of 25° is appropriate to observe
83 soil moisture [Singh, 2005]. For the TerraSAR-X sensor, Paris Anguela et al. (2010) have found
84 that the sensitivity of the radar signal to soil moisture is approximately 0.35 dB/% for the HH-25°
85 configuration.

86 The surface area of soil particles in a soil depends on the particle sizes which control the
87 percentage of free and bound water [Srivastava et al., 2009]. Few studies have analyzed the
88 response of the radar signal to soil composition in terms of grain-size distribution (percentages of
89 sand and clay), but several studies have evaluated the effect of salt content on the radar signal.
90 These studies have underlined the influence of salt concentrations on dielectric properties [Aly et

91 al., 2007; Lasne et al., 2008; Shao et al., 2003; Taylor, 1996]. Several studies have recommended
92 high radar wavelengths (L-band) and wet soil conditions for better discrimination between saline
93 and non-saline soil. Under the wettest conditions (soil moisture greater than 30%), the effects of
94 salinity on the C-band are important for sandy soil but do not appear clearly in soils of finer
95 composition due to salt retention by fine particles, such as silt and clay [Aly et al., 2007]. Also,
96 grain-size distribution has an effect on dielectric behavior over the entire frequency range (1.4 to
97 18 GHz) and is most pronounced at frequencies below 5 GHz [Hallikainen et al., 1985]. In the C-
98 band, decreasing soil clay content increases the sensitivity of the radar signal to soil moisture (0.22
99 dB/% for clay soil: 49% clay, 35% silt and 16% sand; 0.33 dB/% for loamy soil: 17% clay, 48%
100 silt and 35% sand) [Ulaby et al., 1978]. Because the distribution of grain sizes controls the amount
101 of free water that interact with the incident microwave, the amount of free water gives significant
102 contribution to SAR backscatter [Srivastava et al., 2006, 2009]. Recent methodology developed to
103 retrieve soil moisture is based on this amount of free water which is controlled by the grain size
104 distribution [Srivastava et al., 2009].

105 In the X-band at HH polarization, Prakash et al. (2009) have shown a relationship between the
106 specular scattering coefficient for bistatic scatterometer data and the sand percentage in the soil
107 when surface roughness is less than 1.4 cm. For the TerraSAR-X sensor, Paris Anguela et al.
108 (2010) have also shown (based on one plot and one SAR acquisition at HH-25°) that the SAR
109 signal is 3 dB weaker for a soil composition with more clay (32% clay, 64.5% silt and 3.5% sand)
110 than for a soil with less clay (17% clay, 79% silt and 4% sand).

111 Because soil slaking depends primarily on material properties (moisture, organic-matter content
112 and carbonate content) and decreases infiltration rates, the backscattered radar signal may be
113 sensitive to this soil parameter. Nevertheless, few studies have examined the effect of soil slaking
114 on the radar signal. In the X-band, Stolp & Janse (1986) have carried out a multiple linear
115 regression to relate the backscattering coefficient (HH-15°) to the degree of slaking, the direction

116 of tillage and the incidence angle. Their results are promising and provide good estimates of the
117 degree of slaking (with an accuracy between 78% and 56%).

118 Finally, soil parameters are usually estimated from SAR imagery at plot or watershed scales. Few
119 studies have been conducted at the within-plot scale. In fact, the speckle effects and low resolution
120 (between 10 and 30 m) of the first-generation SAR data (ERS, RADARSAT-1 and ASAR)
121 prevented the analysis of small-scale variations. The high spatial resolution of the TerraSAR-X
122 sensor (1 m) provides access to soil-surface heterogeneities at a finer scale. Baghdadi et al. (2008a)
123 have already mentioned signal variations from TerraSAR-X images within agricultural plots.
124 Quantitative analysis were not conducted, but only observations were given from photo-
125 interpretation of SAR images. Paris Anguela et al. (2010) have made a preliminary diagnostic with
126 an analysis from only one bare agricultural plot and in using only one TerraSAR image. In the
127 present work we consolidated and completed these previous investigations in using large database
128 of in situ measurements (soil composition, soil moisture and observations concerning the presence
129 or the absence of crust) and TerraSAR-X images at different radar incidence angle.

130 The main objective of this study is to analyze the potential of the TerraSAR-X radar sensor to
131 characterize soil-surface parameters at the plot and within-plot scales. The effects of soil moisture,
132 roughness, soil composition and slaking crust on the TerraSAR-X backscattering coefficient are
133 analyzed only over agricultural plots.

134

135 **2. MATERIAL AND METHODS**

136 **2.1. STUDY SITE**

137 The study site is the Orgeval watershed (104 km²), which is located to the east of Paris (France;
138 48°51'N 3°07'E; Figure 1). The site has been managed since 1962 as an experimental basin for
139 hydrological research by the Agricultural and Environmental Engineering Research Center

140 (CEMAGREF) research institute. The Orgeval watershed is mostly composed of agricultural plots
141 intended for growing wheat and maize. It is flat and composed of loamy soils with average
142 percentages of 17% clay, 78% silt, and 5% sand. This soil structure promotes crust development,
143 which increases soil sealing and causes runoff [Boiffin et al., 1990; Eimberck, 1990].

144

145 **2.2. SATELLITE DATA**

146 **2.2.1. SAR data:**

147 Fourteen TerraSAR-X images (X-band) were acquired in 2009 and 2010 in Spotlight mode (pixel
148 spacing ~1 m) with HH polarization and incidence angles of 25° and 50°. The incidence angles of
149 each TerraSAR image are summarized in Table 1.

150 Radiometric calibration of the MGD (Multi Look Ground Range Detected) TerraSAR images was
151 carried out using the following equation [Fritz, 2007]:

$$\sigma^{\circ} = (K_s \cdot DN^2 - NEBN) \cdot \sin(\theta) \quad (1)$$

152 This equation transforms the digital number of each pixel DN (amplitude of the backscattered
153 signal) into a backscattering coefficient (σ°) corrected for sensor noise (NEBN) on a linear scale.
154 This calibration takes into account the radar incidence angle (θ) and the calibration constant (K_s)
155 provided in the image data. The backscattering coefficients are then calculated in decibels by the
156 following formula:

$$\sigma_{dB}^{\circ} = 10 \cdot \log_{10}(\sigma^{\circ}) \quad (2)$$

157 This radiometric calibration makes it possible to perform multi-temporal analysis of the different
158 images. All of the images were then co-registered using aerial orthophotos (50-cm spatial
159 resolution) with a root mean square error of the control points of approximately one pixel (i.e., 1

160 m). This co-registration error was overcome by removing the boundary pixels (two pixels wide)
161 from each training plot relative to the limits defined by the GPS control points.

162

163 **2.2.2. Optical data:**

164 One optical IKONOS image was acquired on March 14, 2009 in multispectral mode (pixel spacing
165 ~ 4 m). The IKONOS image was calibrated for TOA (top of atmosphere) reflectance and co-
166 registered using aerial orthophotos with a root mean square error of the control points of
167 approximately one pixel (i.e., 4 m).

168

169 **2.3. EXPERIMENTAL MEASUREMENTS**

170 Simultaneously to the TerraSAR-X acquisitions, ground measurements were performed in thirteen
171 bare training plots in 2009 and 2010 (\pm three hours around the satellite overpass time) (Figure 2).

172 All training plots were flat (slope < 1%). Four soil-surface parameters were observed or measured:
173 moisture content (at the 0-5-cm depth), surface roughness, soil composition, and slaking crust.

174 Meteorological data (precipitation and temperature) were also obtained from five meteorological
175 stations installed in the basin. Each station is less than 5 km from the center of each plot. Figure 3

176 shows the mean values of meteorological data recorded in 2009 (a) and 2010 (b) at the five

177 stations.

178

179 **2.3.1. Soil roughness (*H_{rms}*):**

180 Measurements of soil roughness were carried out in all of the training plots using 1-m-long needle
181 profilometers with 2-cm sampling intervals. Ten roughness profiles along and across the direction

182 of tillage (five parallel and five perpendicular) were established in each training plot. Two

183 parameters can be calculated from these measurements: the average root mean square surface

184 height (H_{rms}) and the correlation length (L) [Ulaby et al., 1986]. The H_{rms} values of the plots
185 obtained during the two field surveys (March to May 2009 and March 2010) varied between 0.4
186 and 3.9 cm. The lower values (0.4 to 1.5 cm) corresponded to sown plots, whereas the higher
187 values (above 1.5 cm) corresponded to fallow and recently ploughed plots. The correlation length
188 (L) varies from 2.3 cm in sown fields to 9.3 cm in ploughed fields. As shown in Figure 4, the
189 relationship between the H_{rms} and the correlation length can be modeled by a linear regression
190 [Davidson et al. 2003, Baghdadi et al. 2008a]. Nevertheless, inverting the two parameters H_{rms}
191 and L separately in the inversion of radar measurements seems to be a difficult task because our
192 TerraSAR images contain a single band per pixel (one polarization and one incidence angle).
193 The error on the roughness computation is influenced mainly by the roughness profiles length, the
194 number of profiles, and the horizontal resolution (sampling interval) of profiles.
195 According to Oh and Kay (1998), the roughness profiles length should be at least $40L$ and $200L$
196 (where L is the correlation length) in order to obtain the H_{rms} and the correlation length with a
197 precision of 10%. Lievens et al. (2009) and Callens et al. (2006) have demonstrated that shorter
198 profiles result in lower H_{rms} and correlation length. A significant underestimation of roughness
199 parameters is observed for short profiles and large correlation length. The number of averaged
200 profiles that is required to obtain a standard deviation on H_{rms} and L less than 10% is dependent
201 of profile length. Lievens et al. (2009) demonstrated that less than 10 averaged profiles are
202 required for 1 m profile to obtain a standard deviation of H_{rms} lower than 10%, whereas the same
203 accuracy (better than 10%) for correlation length only becomes feasible for at least 15 averaged
204 profiles. The precision on the correlation length measurements should be about 15 to 20% for the
205 range of correlation length measured within our bare agricultural fields, with 1m profile and 10
206 average profiles (higher standard deviation for large correlation length). The precision associated
207 with the measurements of H_{rms} and L , were also dependent on the horizontal spacing between
208 height points (Δx). Oh and Kay (1998) suggested that the surface should be sampled at a spacing

209 no longer than $0.2L$ and no more than $0.5L$ for the same precision of about 5% on the correlation
210 length and the *Hrms* surface height, respectively. For our range of correlation length, the accuracy
211 of roughness parameters with a spacing of 2 cm should be better than $\pm 10\%$ for *Hrms* and
212 between $\pm 10\%$ and $\pm 20\%$ for large and small correlation lengths, respectively. According to
213 Lievens et al. (2009), an increase in horizontal spacing causes a decrease in *Hrms* and an increase
214 in correlation length, which are more pronounced for surfaces with small correlation length.
215 Moreover, the standard deviation of roughness parameters with a spacing of 1.5 cm is better than
216 $\pm 5\%$ for *Hrms* and better than $\pm 15\%$ for correlation length.

217 Also, only the relationship between the *Hrms* surface height and the radar signal was used in this
218 study; ten 1-m-long profiles are not sufficient to estimate L parameter with accuracy lower than
219 15% [Oh & Kay, 1998].

220 Finally, most of our training plots don't have marked row directions because they correspond to
221 old winter ploughed without row direction (isotropic surface).

222

223 **2.3.2. Soil moisture (*mv*):**

224 In most studies of microwave measurements carried out over bare soils, experimental relationship
225 between soil moisture and backscattering coefficient are provided by mean volumetric water
226 contents measured to a soil depth, generally 0-5 cm. At X-band, no experimental measurements
227 were conducted in field condition and the low penetration of this radar wavelength is only based
228 on theoretical study. So, the penetration depth of the X-band is not yet known.

229 In this study, between fifteen and twenty-eight gravimetric soil-moisture samples (depth: 0-5 cm)
230 were collected per day for each training plot. The location of each gravimetric measurement was
231 recorded using a GPS device.

232 All gravimetric measurements were converted into volumetric moisture (mv) based on bulk
233 density. Five bulk-density measurements were made for each training plot using 9-cm-long
234 cylindrical samples with volumes of 500 cm^3 . Bulk-density values varied between 0.9 and 1.4
235 g.cm^{-3} . The soil moisture of each plot (or part of a plot) was assumed to be equal to the mean value
236 estimated from the samples collected in that plot (or part of a plot). The two field surveys in 2009
237 and 2010 covered a large range of soil moisture, between 12.6% and 39.8% (see Table 1). The
238 standard deviation of soil moisture measurements varied between 0.6% and 2.75% per each
239 training plot (or part of a plot).

240

241 **2.3.3. Soil composition:**

242 Soil composition was analyzed only in the training plots studied in 2009. For each training plot,
243 ten soil samples were analyzed for their percentages of clay, sand and silt. The analysis showed
244 that the surface soils within the training plots could be classified into two categories of loam:

245 - soil I: clay = $24\% \pm 1.9\%$; silt = $71\% \pm 1.7\%$; sand = $5\% \pm 1.5\%$.

246 - soil II: clay = $16\% \pm 0.9\%$; silt = $78\% \pm 2\%$; sand = $6\% \pm 1.3\%$.

247 The major differences between these two soils corresponded to small variations in clay and silt
248 content (clay = 8%, silt = 7%). The largest difference in clay content between soil I and soil II was
249 found in plot D (~10%), and the smallest value was found in plot G (~3%). The differences in sand
250 content were very small (mean ~1%).

251

252 **2.3.4. Slaking crust:**

253 The structure of bare soils can be modified by the energy of impact of raindrops, and a slaking
254 crust can be formed on the soil surface. A slaking crust decreases the infiltrability of the soil,

255 favoring runoff. This phenomenon is commonly observed on loamy soils and is dependent on soil
256 composition (clay and silt content, organic matter and carbonate content).

257 The presence or absence of slaking crust on the soil surface was noted during the 2009 field
258 survey. Slaking crust blocks the porosity of the soil surface, creating a layer of compacted soil that
259 is often visible to the naked eye. The stagnation of water and the presence of a thin, continuous
260 and consistent surface layer (crust) indicate the spatial extent of the slaking crust.

261 In March 2009, we observed slaking crust with a thickness of approximately 1 cm on soil II
262 ($16\% \pm 0.9\%$ clay, $78\% \pm 2\%$ silt and $6\% \pm 1.3\%$ sand). In April and May 2009, no slaking crusts
263 were observed within the training plots due to tillage operations that had removed the soil crusts
264 and increased the porosity of the topsoil.

265

266 **3. RESULTS**

267 **3.1. TERRASAR-X SIGNAL AND SOIL-SURFACE ROUGHNESS**

268 For bare soils, surface roughness plays an important role in the amount of energy returned to the
269 radar instrument. The sensitivity of the TerraSAR-X signal (σ°) in HH polarization to surface
270 roughness ($Hrms$) at the plot scale was analyzed for both incidence angles (25° and 50°). The
271 database was classified into three soil-moisture groups: $10\% < m_v < 15\%$ (low), $15\% < m_v < 25\%$
272 (medium) and $25\% < m_v < 40\%$ (high). For each incidence angle and soil-moisture group, the
273 relationship between σ° and $Hrms$ was analyzed.

274 For high soil moisture, σ° could be modeled by a logarithmic function according to $Hrms$ for either
275 incidence angle (Figures 4a and 4b), and σ° was more sensitive to surface roughness at a high
276 incidence angle (50°) than at a low incidence angle (25°). The mean difference between the σ°
277 values of the smoothest ($Hrms = 0.7$ cm) and roughest areas ($Hrms = 3$ cm) reached a maximum of
278 1.9 dB at 25° (Figure 5a) and approximately 3.5 dB at 50° (Figure 5b). Similar dynamics of the

279 TerraSAR-X signal and surface roughness have been observed by Baghdadi *et al.* (2008a).
280 Moreover, at an incidence angle of 25° , the backscattering coefficient quickly reaches its
281 maximum level for an *Hrms* of approximately 0.8 cm (Figure 5a). Beyond this threshold, the
282 backscattering coefficient becomes constant regardless of the roughness. Roughness values of less
283 than 0.8 cm are rare in agricultural areas. Therefore, for agricultural applications, soil-roughness
284 mapping is not feasible using X-band SAR data at a low incidence angle.

285 For medium soil moisture, the backscattering coefficient was almost constant for *Hrms* surface
286 heights between 1.1 and 2.7 cm at either incidence angle (Figures 4a and 4b).

287 The lack of roughness data for low soil-moisture conditions made it possible to perform only
288 partial observations for the 50° incidence angle. As observed for medium soil moisture, σ° values
289 for low soil moisture seem to be independent of surface roughness for *Hrms* surface heights
290 between 1.1 and 2.7 cm (Figure 5b).

291 The backscattering coefficients of soils with the same roughness but different soil-moisture levels
292 (medium and high) were also compared. At a 25° incidence angle and for *Hrms* values between
293 1.1 and 2.7 cm, the backscattering coefficient of a soil with medium moisture content was
294 approximately 4.0 dB lower than that of the same soil with high moisture content (Figure 5a). This
295 difference of 4.0 dB was larger than that observed between smooth (*Hrms* \sim 0.4 cm) and rough
296 (*Hrms* \sim 3 cm) soils (1.9 dB). At a 50° incidence angle and for *Hrms* surface heights between 0.8
297 and 2.7 cm, the backscattering coefficient of a soil with medium moisture content was
298 approximately 1.5-5 dB lower than that of the same soil with high moisture content (Figure 5b).

299 The difference in the backscattering coefficient between soils with different levels of moisture was
300 smaller than the dynamics of the backscattering coefficient with changes in roughness at high soil
301 moisture (3 dB for *Hrms* values between 0.8 and 2.7 cm, Figure 5b) for the smoothest areas and
302 larger for the roughest areas. The lack of roughness data with low moisture content made it
303 possible to perform only partial observations. At a 50° incidence angle and for *Hrms* values

304 between 1.2 and 2.9 cm, the backscattering coefficient for low soil moisture was lower by
305 approximately 4-6 dB than that of soils with high soil moisture (Figure 5b). This difference was
306 larger than the difference in backscattering coefficient between soils with different levels of
307 roughness at high soil moisture (2.1 dB for *Hrms* between 1.2 cm and 2.9 cm, Figure 5b).

308 In conclusion for agricultural bare plots, the effects of soil roughness on the TerraSAR-X signal
309 are small and function of the moisture content. Consequently, the backscattering coefficient σ°
310 (dB) in the X-band cannot be expressed as the sum of one function dependent on soil moisture and
311 another dependent on *Hrms* surface height, as is commonly assumed for the L- and C-bands
312 [Baghdadi et al., 2006; Zribi & Deschambre, 2002].

313

314 **3.2. TERRASAR-X SIGNAL AND SOIL MOISTURE CONTENT**

315 The high spatial resolution of the TerraSAR data (1 m) made it possible to analyze the radar signal
316 according to soil moisture at the plot and within-plot scales. The mean backscattering coefficient
317 was estimated for each training plot according to the scale of interest and plotted as a function of
318 in situ soil-moisture measurements regardless of roughness. Figure 6 illustrates the dynamics of
319 the radar backscattering coefficient versus soil moisture for HH polarization at low (25°) and high
320 (50°) incidence angles. Overall, the scattering behavior of the soil increased with soil moisture.
321 The wide range of soil-moisture measurements (13-40%) made it possible to establish linear
322 relationships between the radar signal and the soil moisture for each incidence angle. The
323 sensitivity of the radar signal to soil moisture was 0.411 dB/% for the TerraSAR-X data at 25°
324 (Figure 6a). Paris Anguela et al. (2010) have observed a sensitivity of the same order using a
325 single TerraSAR-X image and simulated data from the IEM model (X-HH-26°: 0.35 dB/%). For
326 the high incidence angle (50°), the sensitivity of the TerraSAR-X signal to soil moisture decreased
327 to 0.323 dB/% (Figure 6b). This analysis demonstrates that the SAR signal in the X-band is
328 slightly more sensitive to soil moisture at a low incidence angle (25°), but soil-moisture mapping

329 can be carried out with either low or high incidence angles (because both showed high
330 sensitivities). This decreasing radar sensitivity with increasing incidence angle is consistent with
331 other studies performed using C-band SAR data. Indeed, several studies using C-band data (ERS,
332 RADARSAT, ASAR) have shown higher sensitivities between the radar signal and soil moisture
333 for low incidence angles (0.2-0.3 dB/%) than for high incidence angles (0.1 dB/%) [Baghdadi et
334 al., 2008a; Le Hégarat et al., 2002; Quesney et al., 2000; Srivastava et al., 2003]. Finally, the
335 sensitivity of the radar signal to soil moisture appears to be higher in the X-band than in the C-
336 band, regardless of the incidence angle. Theoretical surface backscattering models show
337 approximately the same sensitivity between radar signal and soil moisture for these two radar
338 wavelengths (Fung, 1994). The increasing in the sensitivity of radar signal to soil moisture at X-
339 band could be due particularly to volume scattering effect. First, radar signal increases with soil
340 moisture for C- and X-bands. In the other hand, the volume scattering term is certainly higher at C-
341 band than at X-band for low and medium moistures due to more important penetration of waves.
342 This means that at C-band, the dynamic of radar signal with soil moisture variation could be lower
343 at C-band because of this scattering term added for low and medium soil moistures. This decrease
344 in radar dynamic induces a decreasing of sensitivity at C-band.

345

346 **3.3. TERRASAR-X SIGNAL AND SOIL COMPOSITION**

347 The sensitivity of the TerraSAR-X signal to soil composition was studied using images acquired in
348 2009 because the soil-composition analysis focused on the training plots measured in 2009.

349 Heterogeneities within plots were observed in the TerraSAR-X images only on March 17 and 18,
350 2009 (Figures 2 and 7). These variations within the training plots were also observed in the
351 IKONOS image (Figure 7j).

352 To investigate these differences, soil samples were taken in each training plot to determine the
353 particle-size distribution within plots. According to the soil-composition analysis, the zones with

354 low radar-signal values (darker zones) were more clayey (soil I: 24% clay, 71% silt and 5% sand)
355 than the zones with high radar-signal values (brightest zones; soil II: 16% clay, 78% silt and 6%
356 sand). Also, the variations in the TerraSAR-X signal within plots were spatially correlated with the
357 variations in soil composition on the two acquisition dates (March 17 and 18).

358 The mean differences in σ° between soil-II zones and soil-I zones had the same order of magnitude
359 for the HH-25° (March 17: 2.6 dB) and HH-50° (March 18: 2.3 dB) configurations. Indeed, these
360 two acquisitions occurred within an interval of less of 24 hours (ensuring the same surface
361 conditions). Thus, according to these observations, the TerraSAR-X data allow to map limits of
362 our two soils within the plots regardless of the incidence angle.

363 Simulations using the IEM radar-backscattering model [Fung, 1994] were also carried out for the
364 two soil compositions (I and II). The surface-roughness (H_{rms} , l) and soil moisture (mv) values
365 measured during the field survey were used to run the simulations. In the IEM model, the
366 Hallikainen equations [Hallikainen et al., 1985] are used to calculate the dielectric constant
367 according to the percentages of sand and clay. Our results showed that the X-band data did not
368 discriminate the two soil categories (the variations between these soil categories were less than 1
369 dB in the X-band). These results were expected because the difference in soil composition between
370 soil categories II and I was small. Indeed, the two soil compositions measured within the plots had
371 a maximum mean difference in clay content of approximately 10% (training plot D). Several
372 studies in the C- and L-bands have shown that the radar signal is directly dependent on the amount
373 of sand and clay, but only for soil compositions that are very different (differences in clay content
374 of more than 30%) [Dobson & Ulaby, 1981; Schmugge et al., 1976; Ulaby et al., 1978].

375 Similarly, the mean differences in sand content between the two soil categories did not exceed 1%.
376 Prakash et al. (2009) has shown that the specular-scattering coefficient of X-band bistatic
377 scatterometer data at HH polarization is strongly dependent on the percentage of sand in the soil
378 when the surface is smooth. The change in the specular-scattering response with variations in soil

379 composition is difficult to observe when the soil is rough ($Hrms > 1.4$ cm). On March 2009, the
380 smoothest training plots had a roughness of approximately 1.9 cm. Therefore, changes in
381 scattering with changes in soil composition within our rough plots were not clear in the TerraSAR
382 data.

383 Thus, the TerraSAR-X signal was not directly sensitive to the soil composition in our training
384 plots. Nevertheless, the spatial variation in the TerraSAR signal at the within-plot scale was
385 correlated with the spatial distribution of soil composition in some TerraSAR-X acquisitions.
386 Therefore, soil composition should affect other soil parameters that directly influence the
387 TerraSAR-X signal.

388

389 **3.4. TERRASAR-X SIGNAL AND SOIL CRUST**

390 During the field survey in March 2009, slaking crust was observed on soil II and not on soil I. We
391 studied the effect of the soil-II crust on the radar signal for seven training plots of 2009. Because
392 soil crusts modify the water-retention properties and infiltration rates of the soil [Augeard, 2006;
393 Musy & Soutter, 1991], the differences in soil moisture between soil II and soil I ($mv_{soil II} - mv_{soil I}$)
394 were compared to the differences in the TerraSAR signal ($\sigma^{\circ}_{soil II} - \sigma^{\circ}_{soil I}$). The acquisitions on
395 March 17 and 18, 2009 differed from the other 2009 acquisitions by their greater variation in
396 signal and soil moisture within the training plots. The mean difference in signal calculated from
397 the March 17 and March 18 images between the soil-II and soil-I zones was approximately +2.5
398 dB (Table 3) for a mean difference in moisture content of approximately +4.5% (2.9-7.2%,
399 depending on the training plot) (Table 2). The difference in soil moisture between soils I and II can
400 be explained by the difference in the soil-surface structure (i.e., the presence or absence of slaking
401 crust). During the winter dry period (March 11 to March 22, Figure 3), soil I dries faster than soil
402 II. In soil II, evaporation is limited by the crust, and the moisture content is retained longer than in
403 soil I. Thus, the moisture-content values of soil I were lower than those of soil II. Because the

404 TerraSAR signal is highly sensitive to soil moisture (section 3.2), the variations in moisture
405 content between the two soils generated differences in the backscattered signal.

406 On March 25 and 26, the mean difference in signal between soil-II and soil-I zones was less than 1
407 dB (Table 3) for an average difference in moisture content of less than 1% (Table 2). Thus, no
408 variation in either soil moisture or TerraSAR-X signal was observed within the plots on these
409 dates. After rainy events (2.7 mm on March 23 and 4.7 mm only three hours before the March 25
410 acquisition; Figure 3), the moisture content of soil I increased strongly (by approximately +4.5%)
411 because soil I absorbed both precipitation and streaming water coming from soil II. The moisture
412 content of soil II increased slightly (by approximately 1%) because the soil crust prevented water
413 infiltration and favored hydric inertia. On March 17 and 18, soil II had greater moisture content
414 than soil I. Because the moisture content of soil I increased and the moisture content of soil II
415 stayed constant, the difference in moisture content between the two soils disappeared. For the
416 other acquisition dates between April 8 and May 11, 2009, tillage had destroyed the soil crust and
417 increased the porosity of soil II. Without crust, the compositions of the two soils were too similar
418 to generate a difference in moisture content between soil I and soil II ($< 1\%$), and no differences in
419 signal were observed between the two soils.

420 Thus, variations in the TerraSAR-X signal within plots were correlated with differences in the
421 soil-surface structure between the two soils. The slaking crust on soil II generated differences in
422 moisture content between soil I and soil II under certain conditions. For a single training plot
423 located within the same study area, Paris Anguela et al. (2010) have shown that a soil with a
424 smaller percentage of clay (soil B: 17% clay, 79% silt and 4% sand) had a TerraSAR signal (HH-
425 25°) 3 dB stronger than that of a more clayey soil (soil A: 32% clay, 64.5% silt and 3.5% sand).
426 The driest upper millimeters of soil B and the low X-band penetration at high moisture content
427 [Nolan & Fatland, 2003] were used to explain the difference in signal between soil B and soil A.

428

429 4. CONCLUSIONS

430 This study analyzes the potential of high-spatial-resolution data from the TerraSAR-X sensor to
431 monitor the soil-surface characteristics of bare agricultural soils (roughness, moisture, composition
432 and structure) at plot and within-plot scales. The backscattering coefficients obtained from multi-
433 temporal SAR acquisitions at HH polarization and two incidence angles (25° and 50°) were
434 compared to ground observations and measurements. Our results are promising for retrieving soil
435 moisture information from TerraSAR-X data and for monitoring the dynamics of slaking crust
436 hydric states within plots. The results are summarized below.

- 437 ➤ For high soil moisture ($25 < m_v < 40\%$), the sensitivity of the TerraSAR-X backscattering
438 coefficient to soil roughness is slightly higher at a 50° incidence angle (3.5 dB) than at a
439 25° incidence angle (1.9 dB). Moreover, for either incidence angle, the variation in the
440 radar signal with surface roughness is smaller for soils with moisture contents between
441 15% and 25% than for soils with moisture contents over 25%. The sensitivity of the
442 TerraSAR signal at 25° to soil roughness for areas with high moisture content ($25\% < m_v$
443 $< 40\%$) is lower than the difference in signal between two areas with different moisture
444 contents ($15\% < m_v < 25\%$ and $25\% < m_v < 40\%$). At 50°, the change in σ° with surface
445 roughness for high soil moisture is larger than the variation in the signal between two
446 smooth soils ($H_{rms} \sim 0.8$ cm) with different soil moisture levels ($15\% < m_v < 25\%$ and
447 $25\% < m_v < 40\%$) and is slightly smaller in the case of rough areas ($H_{rms} \sim 2.7$ cm).
448 Therefore, in the X-band, a high incidence angle (50°) is the optimal configuration for soil-
449 roughness monitoring in agricultural areas (bare soils).
- 450 ➤ The sensitivity of the TerraSAR-X signal to soil moisture is greater at a low incidence
451 angle than at a high incidence angle (25°: 0.411 dB/%; 50°: 0.323 dB/%). Thus, an increase
452 in moisture content of approximately 5% generates an increase in the backscattered signal
453 of approximately 2.0 dB at a 25° incidence angle and 1.6 dB at a 50° incidence angle.

454 ➤ The X-band SAR signal is not sensitive to slight differences in soil composition in bare
455 agricultural fields (the maximum differences in our plots were 10% in clay and 1% in
456 sand). No direct influence of soil composition on the radar signal was observed.
457 Nevertheless, two TerraSAR-X acquisitions have shown signal variations within reference
458 plots in the Orgeval study site that are spatially correlated with differences in soil
459 composition at both high (50°) and low (25°) incidence angles (March 17 and 18, 2009).
460 No TerraSAR-X signal variations were observed without crust or when there were no
461 contrast of soil moisture between the soil crusted (II) and not crusted (I). So, when
462 variations of composition engender variations of soil moisture (due to variations of soil
463 structure and meteorological conditions), the spatial extent of soil composition can be
464 observed within plots on TerraSAR-X signal.

465 ➤ Variations in the TerraSAR-X signal within reference plots are correlated with the hydric
466 evolution of soil crust. Soil with slaking crust (soil II) has a greater hydric inertia than soil
467 without crust (soil I). Consequently, following rainfall or dry events, soil moisture in the
468 upper centimeters may differ between the two soil structures, resulting in variations in the
469 TerraSAR-X signal within the field. Thus, it is sometimes possible to track surface
470 degradation due to the slaking process using the TerraSAR-X sensor.

471 Because of the low sensitivity to surface roughness and the high sensitivity to soil moisture, the
472 use of TerraSAR-X data at HH polarization with a single incidence angle is a promising method
473 for estimating soil parameters. Further studies are needed to analyze the complementary
474 polarizations and incidence angles. Similarly, the synergy between the X-band (TerraSAR-X) and
475 other SAR wavelengths (PALSAR/ALOS, RADARSAT-2, ASAR/ENVISAT) should be
476 examined.

477

478 **Acknowledgments**

479 The authors wish to thank DLR (the German Space Agency) for kindly providing the TerraSAR-X
480 images (proposal HYD0007 and HYD0542). We extend our thanks to Noveltis and CNES (the
481 French Space Study Center), which financed this study. We also thank S. Follain for helping to
482 interpret the soil results, Elie Saba for helping to compute IEM simulation and P. Ansart, G. Tallec
483 and Y. Hachouch for helping to collect field data.

484

485 **References**

486 **Aly, Z., Bonn, F. J., Magagi, R. (2007).** Analysis of the backscattering coefficient of salt-affected
487 soils using modeling and radarsat-1 SAR data. *IEEE Transactions on Geoscience and Remote*
488 *Sensing, vol. 45, n° 2: 332 – 341*

489 **Augeard, B. (2006).** Mécanismes de genèse du ruissellement sur sol agricole drainé sensible à la
490 battance. Etudes expérimentales et modélisation. *Doctorat Sciences de l'eau, Unité de Recherche*
491 *Hydrosystèmes et Bioprocédés, ENGREF 06ENGR0010, 236 p.*

492 **Auzet, A.V., Kirkby, M.J., Van Dijk, P. (2005).** Surface characterisation for soil erosion
493 forecasting. *Catena, vol. 62, n° 2–3: 77–78.*

494 **Baghdadi, N., Gaultier, S., King, C. (2002).** Retrieving surface roughness and soil moisture from
495 SAR data using neural network. *Canadian Journal of Remote Sensing vol. 28, n° 5: 701–711.*

496 **Baghdadi, N., Holah, N., Zribi, M., (2006).** Soil moisture estimation using multi-incidence and
497 multi-polarization ASAR SAR data. *International Journal of Remote Sensing, vol. 27, n° 10:*
498 *1907–1920.*

499 **Baghdadi, N., Aubert, M., Cerdan, O., Franchistéguy, L., Viel, C., Martin, E., et al. (2007).**
500 Operational mapping of soil moisture using synthetic aperture radar data: application to Touch
501 basin (France). *Sensors Journal, vol. 7: 2458–2483.*

- 502 **Baghdadi, N., Zribi, M., Loumagne, C., Ansart, P., & Paris Anguela, T. (2008a).** Analysis of
503 TerraSAR-X data and their sensitivity to soil surface parameters over bare agricultural fields.
504 *Remote sensing of Environnement, vol. 112, n° 12: 4370-4379.*
- 505 **Baghdadi, N., Cerdan, O., Zribi, M., Auzet, V., Darboux, F., El Hajj, M., et al. (2008b).**
506 Operational performance of current synthetic aperture radar sensors in mapping soil surface
507 characteristics: application to hydrological and erosion modelling. *Hydrological Processes, vol.*
508 *22, n° 1: 9–20.*
- 509 **Beaudoin, A., Gwy, Q.H.J., Le Toan, T. (1990).** SAR observation and modelling of the C-band
510 backscatter variability due to multi-scale geometry and soil moisture. *IEEE Transactions on*
511 *Geoscience & Remote Sensing, vol. 28: 886-894.*
- 512 **Boiffin, J., Papy F., & Eimberck, M. (1988).** Influence des systèmes de culture sur les risques
513 d'érosion par ruissellement concentré : Analyse des conditions de déclenchement de l'érosion.
514 *Agronomie, vol. 8: 663-673.*
- 515 **Callens, M., Verhoest, N., Davidson, M. (2006).** Parametrization Condition for precise
516 measurement of soil surface roughness. *IEEE Transactions on Geoscience and Remote Sensing,*
517 *vol. 36, n° 2: 691 – 695.*
- 518 **Cerdan, O., Poesen, J., Govers, G., Saby, N., Le Bissonnais, Y., Gobin, A., Vacca, A.,**
519 **Quinton, J., Auerswald, K., Klik, A., Kwaad, F.J.P.M., Roxo, M.J. (2006).** Sheet and rill
520 erosion rates in Europe. *In soil Erosion in Europe, Boardman J., Poesen J (eds), chap. 38. Wiley :*
521 *Chichester, UK: 501–513.*
- 522 **Davidson, M., Mattia, F., Satalino, G., Verhoest, N., Le Toan, T., Borgeaud, M., Louis, J.,**
523 **Attema, E. (2003).** Joint statistical properties of RMS height and correlation length derived from
524 multisite 1-m roughness measurements. *IEEE Transactions on Geosciences and Remote Sensing,*
525 *vol. 41: 1651-1658.*

- 526 **Dobson, M.C., & Ulaby, F.T. (1981).** Microwave backscatter dependence on surface roughness,
527 soil moisture and soil texture: Part III- soil tension. *IEEE Transactions on Geosciences and*
528 *Remote Sensing, vol. 19: 51-61.*
- 529 **Dobson, M.C., & Ulaby, F.T. (1986).** Active microwave soil moisture research. *IEEE*
530 *Transactions on Geoscience and Remote Sensing, vol. GE-24, n° 1: 23-36.*
- 531 **Eimberck, M. (1990).** Facteurs d'érodibilité des sols limoneux: réflexions à partir du Pays de
532 Caux. Cah. (In French.). *ORSTOM, série Pédologique, vol. XXV, n° 1-2: 81-94.*
- 533 **Fung, A.K., & Chen, K.S. (1992).** Dependence of the surface backscattering coefficients on
534 roughness, frequency and polarization states. *International Journal of Remote Sensing, vol. 13:*
535 *1663-1680.*
- 536 **Fung, A.K. (1994).** Microwave Scattering and Emission Models and their Applications. *Artech*
537 *House, Norwood, Massachussetts : 573 p.*
- 538 **Fritz, T. (2007).** TerraSAR-X Level 1b Product Format Specification", *TX-GS-DD-3307, n° 1.3.*
- 539 **Govers, G., Takken, I., Helming, K. (2000).** Soil roughness and overland flow, *Agronomie, vol.*
540 *20: 131-146.*
- 541 **Hallikainen, M., Ulaby, F., Dobson, F., El Rayes, M., & Wu, L. (1985).** Microwave dielectric
542 behavior of wet soil. Part I : Empirical models and experimental observations, *IEEE Transactions*
543 *on Geoscience and Remote Sensing, vol. 23: 25-34.*
- 544 **Holah, N., Baghdadi, N., Zribi, M., Bruand, A., & King, C. (2005).** Potential of
545 ASAR/ENVISAT for the characterization of soil surface parameters over bare agricultural fields.
546 *Remote Sensing of Environnement, vol. 96, n° 1: 78-86.*
- 547 **King, D., & Le Bissonnais, Y. (1992).** Rôle des sols et des pratiques culturelles dans l'infiltration
548 et l'écoulement des eaux . Exemple du ruissellement et de l'érosion sur les plateaux limoneux du
549 nord de l'Europe. *C. R. Acad. FR., vol. 78, n° 6: 91-105.*

- 550 **Lasne, Y., Paillou, Ph., Ruffié, G., Serradilla, C., Demontoux, F. (2008).** Effect of salinity on
551 the dielectric properties of geological materials: implication for soil moisture detection by means
552 of remote sensing. *IEEE Transactions on Geoscience and Remote Sensing*, vol. 46, n° 6: 1674-
553 1688.
- 554 **Le Bissonnais, Y., & Singer, M.J. (1992).** Crusting, Runoff and erosion Response to soil Water
555 Content and Successive Rainfalls. *Soil Science Society American Journal*, vol. 56: 1898-1903.
- 556 **Le Hégarat Mascle, S., Zribi, M., Alem, F., Weisse, A., & Loumagne, C. (2002).** soil moisture
557 estimation from ERS/SAR data : toward an operational methodology. *IEEE Transactions on*
558 *Geoscience and Remote Sensing*, vol. 40, n° 12: 2647-2658.
- 559 **Lievens, H., Vernieuwe, H., Alvarez-Mozos, J., De Baets, B., Verhoest, N., (2009).** Error in
560 radar-derived soil moisture due to roughness parameterization: an analysis based on synthetical
561 surface profiles. *Sensors Journal*, vol. 9: 1067–1093.
- 562 **Loumagne, C., Michel, C., Normand, M. (1991).** Soil water conditions and forecasting rain
563 water runoff. *Journal of Hydrology*, vol. 123: 1-17.
- 564 **Loumagne, C., Weisse, A., Normand, M., Riffard, M., Quesney, A., Le Hegarat-Mascle, S.,**
565 **Alem, F. (2001).** Integration of remote sensing data into hydrological models for flood
566 forecasting. *Remote Sensing and Hydrology 2000, IASH Red Book Pub.*, n°267, edited by
567 *Brubaker, Ritchie, Rango*: 592-594.
- 568 **Musy, A., et Soutter, M. (1991).** Physique du sol. *Presses Polytechniques et Universitaires*
569 *Romandes, Lausanne, Suisse*, 335p.
- 570 **Nolan, M., & Fatland, D.R. (2003).** Penetration Depth as a DInSAR Observable and Proxy for
571 soil Moisture. *IEEE Transactions on Geoscience and Remote Sensing*, vol. 41, n° 3:532-537.
- 572 **Oh, Y., & Kay, Y.(1998).** Condition for precise measurement of soil surface roughness. *IEEE*
573 *Transactions on Geoscience and Remote Sensing*, vol. 36, n° 2: 691 – 695.

- 574 **Oh, Y. (2004).** Quantitative retrieval of soil moisture content and surface roughness from
575 multipolarized radar observations of bare soil surfaces. *IEEE Transactions on Geoscience and*
576 *Remote Sensing, vol. 42, n° 3: 596 – 601.*
- 577 **Oudin, L., Weisse, A., Loumagne, C., Le Hegarat-Masclé, S. (2003).** Assimilation of soil
578 moisture into Hydrological models for flood forecasting a variational approach. *Canadian Journal*
579 *of Remote sensing, vol. 29, n° 6: 679-686.*
- 580 **Paris Anguela, T., Zribi, M., Baghdadi, N., Loumagne, C. (2010).** Analysis of local variation of
581 soil surface parameters with TerraSAR-X radar data over bare agricultural fields. *IEEE*
582 *Transactions on Geoscience and Remote Sensing vol. 48, n° 2: 874–881.*
- 583 **Prakash, R., Singh, D., Pathak, N.P. (2009).** Microwave specular scattering response of soil
584 texture at X-band. *Advances in Space Research, vol. 44, n° 7: 801–814.*
- 585 **Quesney, A., Le Hegarat-Masclé, S., Taconet, O., Vidal-Madjar, D., Wingneron, J.P.,**
586 **Loumagne, C., & Normand, M. (2000).** Estimation of watershed soil moisture index from
587 ERS/SAR data. *Remote sensing of environment, vol. 72, n° 3: 290-303.*
- 588 **Schmugge, T., Wilheit, T., Webster, W., & Gloerson, P. (1976).** Remote sensing of soil
589 moisture with microwave radiometers-II. *NASA Goddard Space Flight Center, Greenbelt, MD,*
590 *20771. NASA Technical Note TN-D-8321.*
- 591 **Shao, Y., Hu Q., Guo, H., Lu, Y., Dong, Q., Han, C. (2003).** Effect of dielectric properties of
592 moist salinized soils on backscattering coefficients extracted from RADARSAT image. *IEEE*
593 *Transactions on Geoscience and Remote Sensing, vol. 41: 1879 – 1888.*
- 594 **Shi, J., Wang, J., Hsu, A.Y., O’Neill, P.E., Engman, E.T. (1997).** Estimation of bare surface soil
595 moisture and surface roughness parameter using L band SAR image data. *IEEE Transactions on*
596 *Geoscience and Remote Sensing, vol. 35, n° 5: 1254–1266.*

- 597 **Singh, D. (2005).** A simplistic incidence angle approach to retrieve the soil moisture and surface
598 roughness at X-band. *IEEE Transactions on Geoscience and remote Sensing*, vol. 43, n° 11:
599 2606-2611.
- 600 **Srivastava, H.S., Patel, P., Manchanda, M.L., Adiga, S. (2003).** Use of multiincidence angle
601 RADARSAT-1 SAR data to incorporate the effect of surface roughness in soil moisture
602 estimation. *IEEE Transactions on Geoscience and Remote Sensing*, vol. 41, n° 7: 1638–1640.
- 603 **Srivastava, H.S., Patel, P., Navalgund, R.R., (2006).** Incorporating soil texture in soil moisture
604 estimation from extended low-1 beam mode RADARSAT-1 SAR data. *International Journal of*
605 *Remote Sensing*, vol. 27, n°12-14: 2587– 2598.
- 606 **Srivastava, H.S., Patel, P., Sharma, Y., Navalgund R.R. (2009).** Large area soil moisture
607 estimation using multi-incidence-angle RADARSAT-1 SAR data. *IEEE Transactions on*
608 *Geoscience and Remote Sensing*, vol. 47, n° 8: 2528–2535.
- 609 **Stolp, J., Janse, A.R.P. (1986).** X-band radar backscattering for detecting spatial distribution of
610 soil slaking. *ITC Journal*, vol. 1: 82-87.
- 611 **Taylor, G. R., Mah, H.A., Kruse, F.A., Kierein-Young, K.S., Hewson, R.D., & Bennett, B.A.**
612 **(1996).** Characterization of saline soils using airborne radar imagery. *Remote Sensing*
613 *Environment*, vol. 57: 127 - 142.
- 614 **Ulaby, F.T., Batlivala, P.P., & Dobson, M.C. (1978).** Microwave backscatter dependence on
615 surface roughness, soil moisture, and soil texture: Part I – Bare soil. *IEEE Transactions on*
616 *Geoscience and Remote Sensing*, vol. GE-16, n° 4: 286-295.
- 617 **Ulaby, F.T., Moore, R.K., & Fung, A.K. (1986).** *Microwave Remote Sensing, Active and*
618 *Passive, From Theory to Applications*, vol. 3, *Artech House, Inc., 685 Canton Street, Norwood,*
619 *MA 02062, 1098 p.*

- 620 **Valentin, C., Poesen, J., Li, Y. (2005).** Gully erosion: impacts, factors and control. *Catena* vol.
621 *63, n° 2–3: 132–153.*
- 622 **Valentin, C., & Bresson, L.M. (1992).** Morphology, genesis and classification of surface crusts in
623 loamy and sandy soils. *Geoderma*, vol. 55: 225-245.
- 624 **Wu, Q., Wang, M. (2007).** A framework for risk assessment on soil erosion by water using an
625 integrated and systematic approach. *Journal of hydrology*, vol. 337: 11-21.
- 626 **Zobeck, T.M., & Onstad, C.A. (1987).** Tillage and rainfall effects on random roughness: a
627 review. *Soil & Tillage Research*, vol. 9: 1-20.
- 628 **Zribi, M., Dechambre, M. (2002).** A new empirical model to retrieve soil moisture and roughness
629 from C-band radar data. *Remote Sensing of Environment*, vol. 84: 42–52.
- 630 **Zribi, M., Baghdadi, N., Holah, N., Fafin, O. (2005).** New methodology for soil surface
631 moisture estimation and its application to ENVISAT-ASAR multi-incidence data inversion.
632 *Remote Sensing of Environment*, vol. 96: 485–496.
- 633

633 **Tables and Figures**

634 *Table 1. Characteristics of TerraSAR images and in situ soil-moisture measurements.*

SAR acquisition date dd/mm/yy	Incidence angle	In situ soil moisture (%) [Min; Max]
17/03/09	25°	[24.7; 32.3]
18/03/09	50°	[24.5; 29.8]
25/03/09	50°	[24.1; 31.0]
26/03/09	25°	[23.9; 32.7]
08/04/09	25°	[16.8; 27.5]
09/04/09	50°	[15.2; 26.3]
17/04/09	25°	[14.1; 16.4]
20/04/09	50°	[18.3; 23.9]
11/05/09	25°	[25.8; 31.3]
01/03/10	50°	[33.4; 39.8]
02/03/10	25°	[32.7; 39.0]
04/03/10	25°	[27.3; 34.3]
12/03/10	50°	[12.6; 29.0]
13/03/10	25°	[14.9; 26.3]

635

636

637

638 *Table 2. Variations in soil moisture within the training plots (%). For each date and training plot,*

639 *the difference in soil moisture between soil II and soil I is shown. Slaking crust was observed on*

640 *soil II on March 17, 18, 25 and 26, 2009. N.A.: not available.*

Training plot ID	TerraSAR-X acquisition date (dd/mm/yy)								
	17/03/09 HH-25°	18/03/09 HH-50°	25/03/09 HH-50°	26/03/09 HH-25°	08/04/09 HH-25°	09/04/09 HH-50°	17/04/09 HH-25°	20/04/09 HH-50°	11/05/09 HH-25°
A	N.A.	N.A.	N.A.	N.A.	N.A.	N.A.	1.6	0.1	N.A.
B	N.A.	5.2	N.A.	2.7	0.5	1.4	0.9	0.2	0.2
C	4.7	3.7	0.5	-1.6	-1.4	-0.3	1.0	0.6	1.1
D	5.1	7.2	N.A.	1.0	N.A.	-1.4	0.1	0.4	0.4
E	3.1	2.9	0.2	-1.0	-0.4	0.1	0.1	0.7	N.A.
F	N.A.	N.A.	N.A.	N.A.	N.A.	N.A.	N.A.	N.A.	N.A.
G	N.A.	N.A.	N.A.	N.A.	N.A.	N.A.	0.7	0.9	0.1
Mean ($mv_{soil II} - mv_{soil I}$) of training plots C, D, E	4.3	4.6	0.3	-0.5	-0.6	-0.5	0.4	0.6	0.7

641

642

643

644 *Table 3. Variations in the TerraSAR-X signal within the training plots (dB). For each date and*
645 *training plot, the difference between the radar signal of soil II and that of soil I is shown. Slaking*
646 *crust was observed on soil II on March 17, 18, 25, and 26, 2009. N.A.: not available.*

Training plot ID	TerraSAR-X acquisition date (dd/mm/yy)								
	17/03/09 HH-25°	18/03/09 HH-50°	25/03/09 HH-50°	26/03/09 HH-25°	08/04/09 HH-25°	09/04/09 HH-50°	17/04/09 HH-25°	20/04/09 HH-50°	11/05/09 HH-25°
A	1.6	1.5	0.5	0.8	0.3	-0.1	-0.2	0.1	1.4
B	2.7	2.1	-2.3	-0.7	0.6	-0.4	-0.5	0.5	-0.6
C	2.4	2.3	-0.1	-0.1	0.4	0.3	0.1	0.7	0.3
D	2.6	2.3	-1.1	0.1	0.7	0.8	-0.5	0.6	-0.2
E	2.8	2.3	-0.4	-0.2	0.8	1.3	N.A.	0.5	0.3
F	2.2	2.6	0.1	-0.4	0.7	0.8	-0.7	N.A.	1.2
G	1.1	1.1	-0.5	0.1	0.7	0.8	-0.1	0.9	0.1
Mean ($\sigma^{\circ}_{soil II} - \sigma^{\circ}_{soil I}$) of training plots C, D, E	2.6	2.3	-0.5	-0.1	0.6	0.8	-0.2	0.6	0.1

647

648

649



650

651 *Figure 1. Location of the Orgeval watershed (France; central coordinates: 48°51'N, 3°07'E).*

652



653

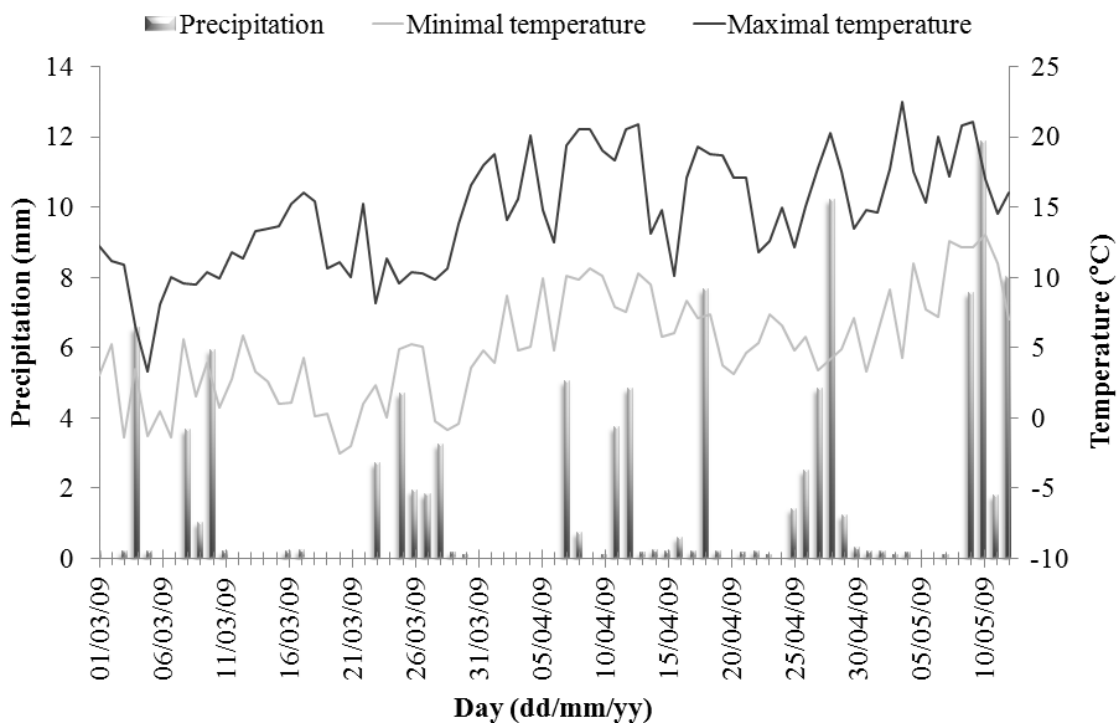
654 *Figure 2. A portion of a TerraSAR-X image (HH-25°, 17 March 2009) of the Orgeval site (central*
655 *coordinates: 48°52'N, 3°06'E). Field surveys were performed in seven plots (A to G) in 2009 and*
656 *six plots (H to M) in 2010. The reference plots are outlined in black.*

657

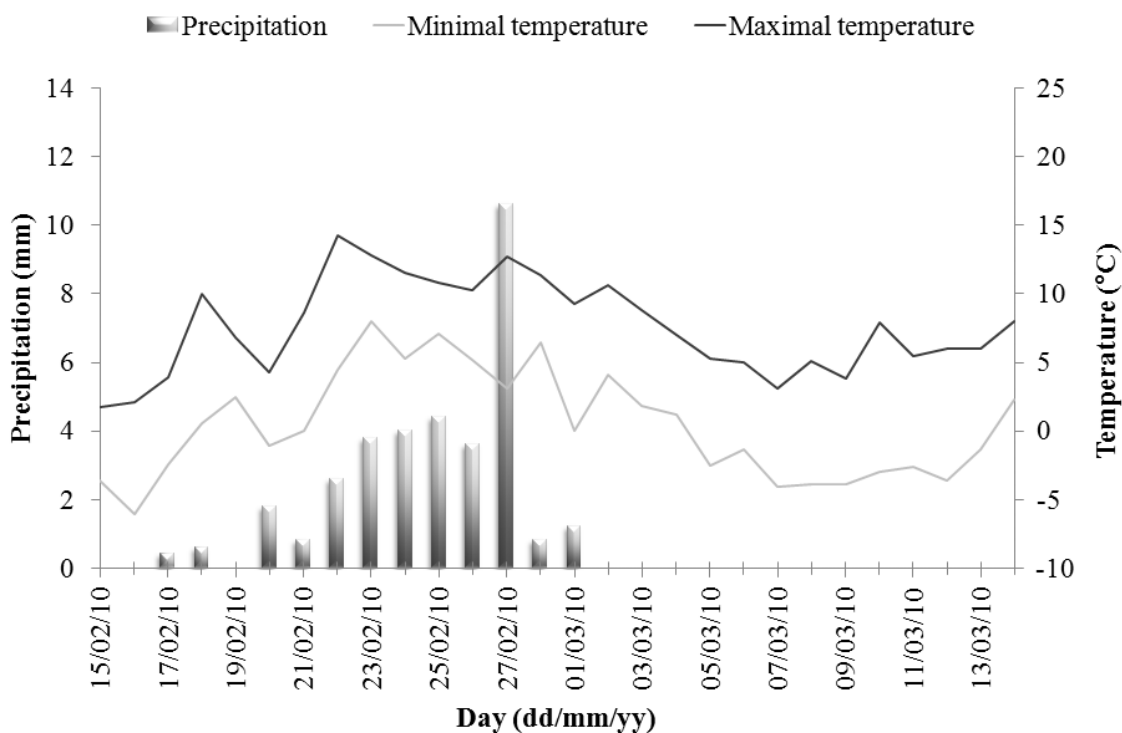
658

659

660



(a)

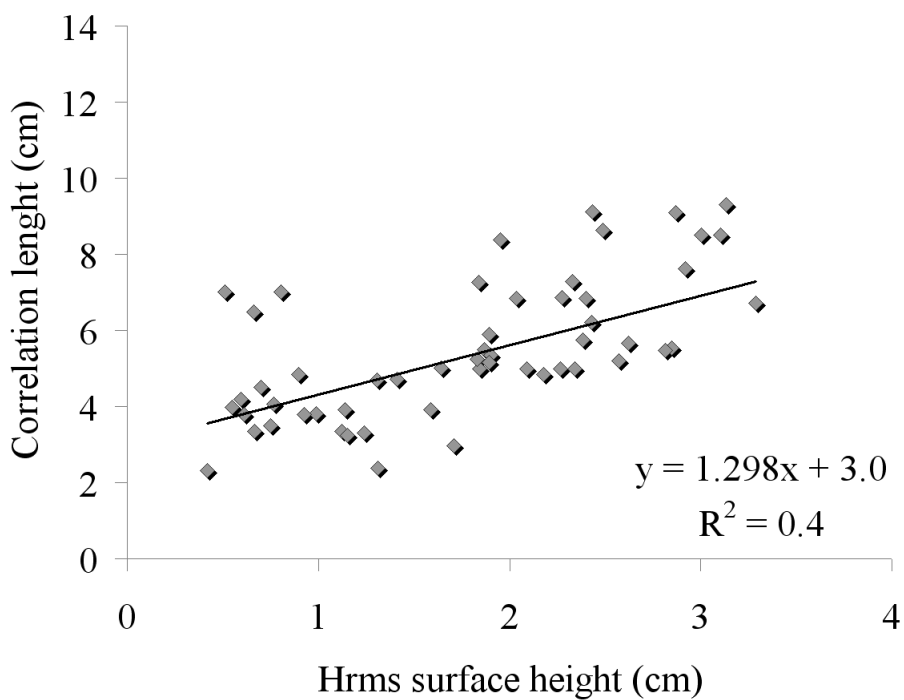


(b)

661

662 *Figure 3. Meteorological data averaged over the five stations installed in the basin: daily*
663 *precipitation (mm) and minimum and maximum temperatures in 2009 (a) and 2010 (b).*

664

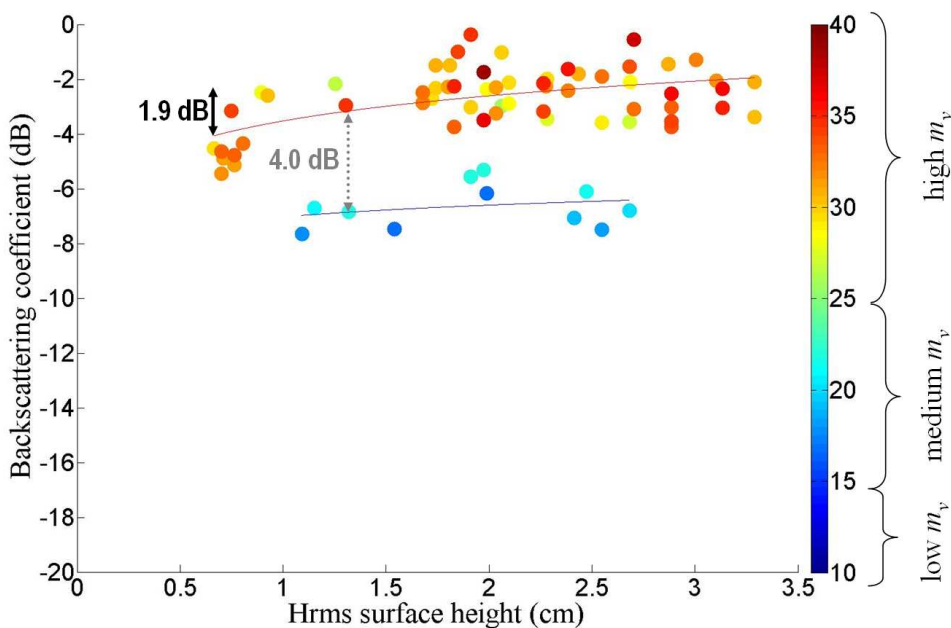


665 *Figure 4. Hrms surface height versus correlation length from measurements carried out in this*

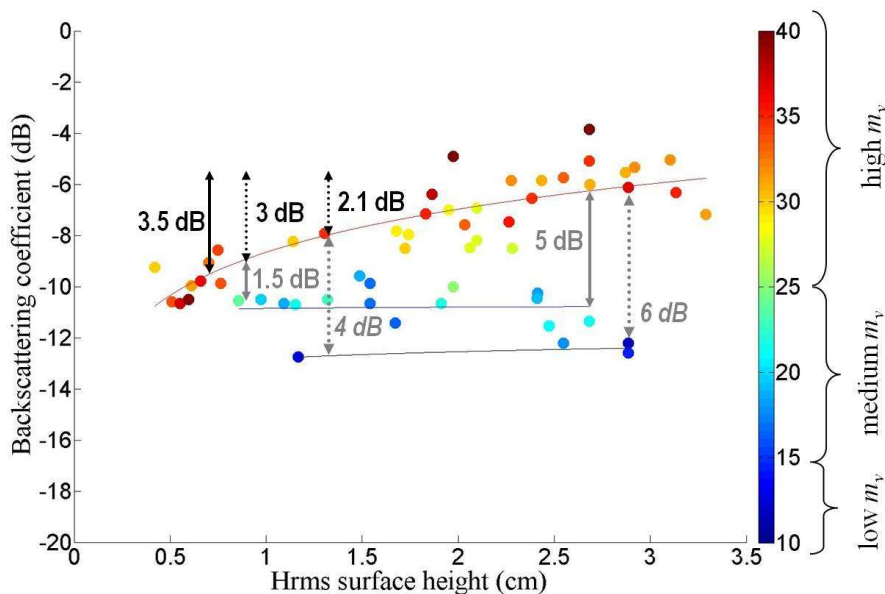
666 *campaign.*

667

667

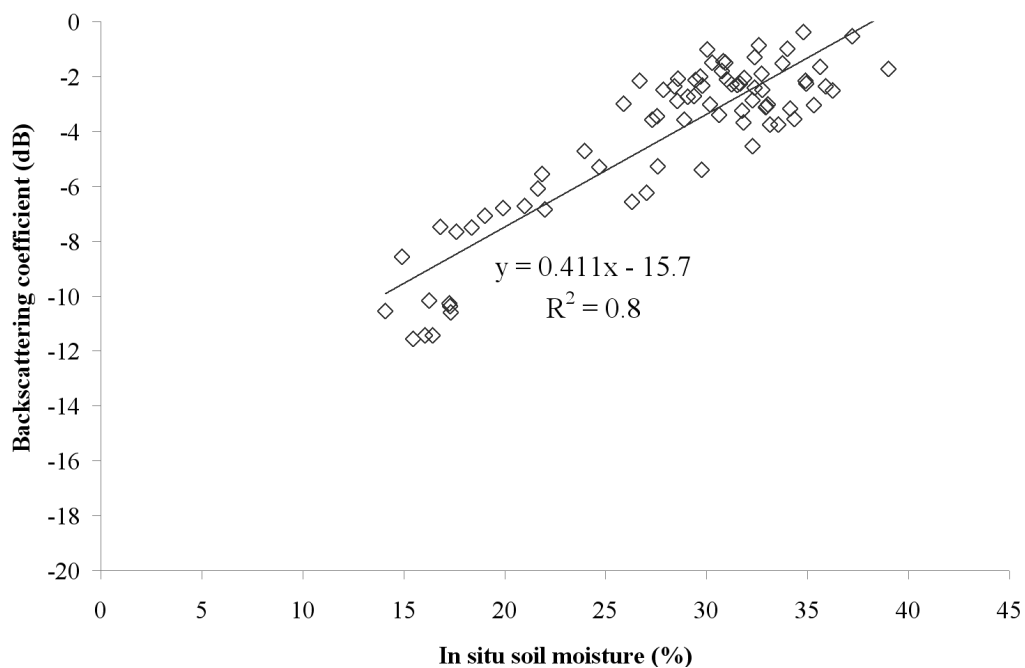


(a) medium m_v : $\sigma^\circ = 0.62 \cdot \ln(Hrms) - 7.0$; $R^2 = 0.1$; RMSE = 0.7 cm
high m_v : $\sigma^\circ = 1.32 \cdot \ln(Hrms) - 3.5$; $R^2 = 0.3$; RMSE = 0.9 cm

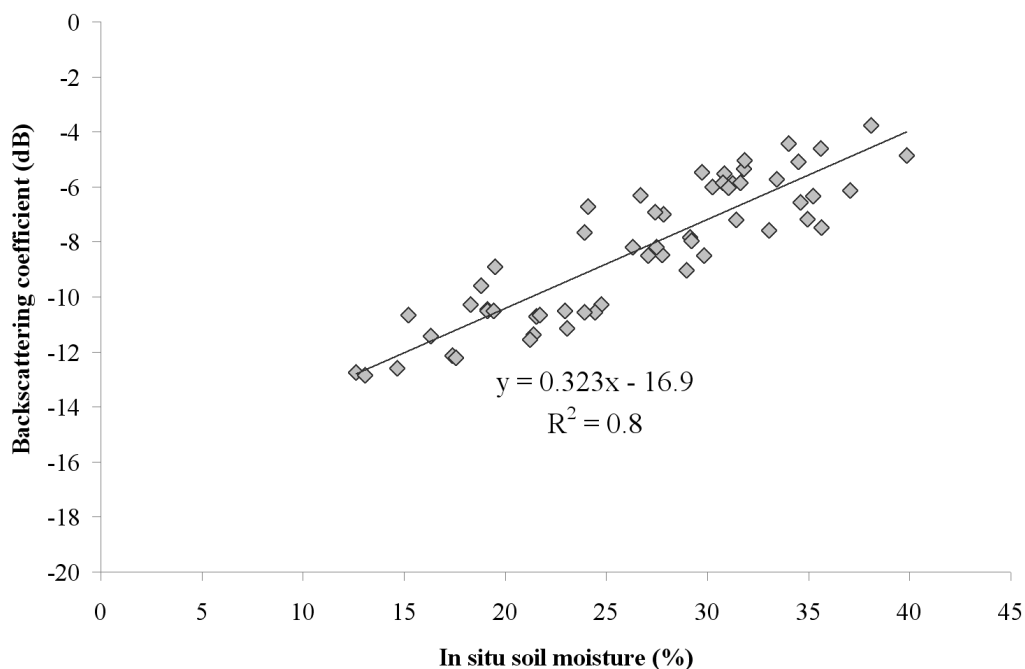


(b) low m_v : $\sigma^\circ = 0.20 \cdot \ln(Hrms) - 12.9$; $R^2 = 0.5$; RMSE = 0.1 cm
medium m_v : $\sigma^\circ = 0.01 \cdot \ln(Hrms) - 10.3$; $R^2 = 0.1$; RMSE = 0.6 cm
high m_v : $\sigma^\circ = 2.43 \cdot \ln(Hrms) - 08.7$; $R^2 = 0.7$; RMSE = 1.0 cm

668 Figure 5. The sensitivity of the TerraSAR-X signal (at HH polarization) to soil roughness for
669 incidence angles of 25° (a) and 50° (b). Each point corresponds to one training plot (mean
670 values).

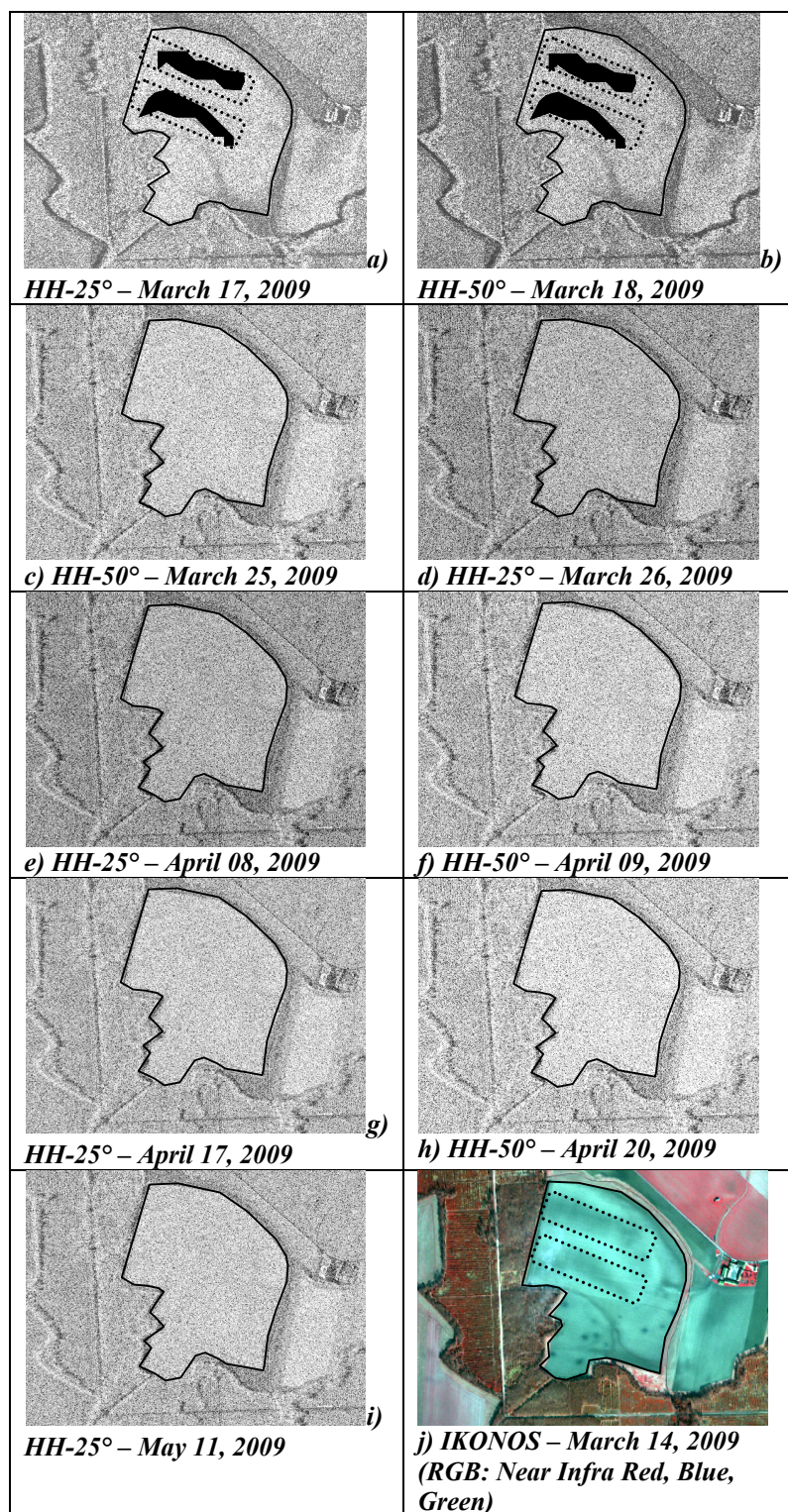


(a) RMSE = 1.32%



(b) RMSE = 1.14%

671 *Figure 6. The sensitivity of the TerraSAR-X signal (at HH polarization) to soil moisture in the top*
672 *0–5-cm soil layer for incidence angles of 25° (a) and 50° (b). Each point corresponds to one*
673 *training plot or portion of a plot.*



674 *Figure 7. Variations in signal strength within training plot C (outlined in black) for each*
675 *TerraSAR-X acquisition (a-i). A subset of the IKONOS image acquired on March 14, 2009 is also*
676 *shown (j). For the 17 and 18 March acquisitions, Soil I is outlined with a dotted black line (darker*
677 *zone), and soil II corresponds to the brighter zones.*